OPEN ACCESS
IOP Publishing
Classical and Quantum Gravity
Class. Quantum Grav. **42** (2025) 155011 (11pp)
https://doi.org/10.1088/1361-6382/adf0e2

A compact triaxial active vibration isolator for cryogenic suspended interferometry

S L Kranzhoff[1,2,*], A Bertolini[1,2], M J C Denissen[3], H L M M Janssen[3], J Lehmann[4,5], B C T van Bree[3], M van Dael[2,6], M Vardaro[1,2] and S Hild[1,2]

[1] Universiteit Maastricht, 6200 MD Maastricht, The Netherlands
[2] Nikhef, Science Park 105, 1098 XG Amsterdam, The Netherlands
[3] JPE, Maastricht-Airport, The Netherlands
[4] Max Planck Institute for Gravitational Physics (Albert Einstein Institute), D-30167 Hanover, Germany
[5] Leibniz Universität Hannover, D-30167 Hanover, Germany
[6] Eindhoven University of Technology, Dept. of Mechanical Engineering, 5612 AE Eindhoven, The Netherlands

E-mail: luise.kranzhoff@ligo.org

Received 11 June 2025; revised 7 July 2025
Accepted for publication 16 July 2025
Published 28 July 2025

Abstract

Suspended interferometry at cryogenic temperatures down to 10–20 K requires conductive cooling in addition to radiative cooling techniques, which is challenging due to vibrations emanating from the ground and direct force perturbations from the cryogenic system potentially acting back on the seismically isolated mirrors. In this work, the passive and active isolation performance of a triaxial cryogenic active vibration isolator designed to operate at temperatures below 10 K and ultra-high vacuum conditions with pressures below 10^{-9} mbar is investigated. While passive isolation of ground motion is effective for frequencies above 6.5 Hz, active suppression of motion and force disturbances can be achieved between 2.46 Hz and 21.4 Hz leading to a reduction of root-mean-square motion by one order of magnitude in the active control band. The performance limits of the current system are evaluated and compared with requirements of ETpathfinder, a prototype facility for investigating cryogenic technologies that enable the target low-frequency sensitivity improvement of

* Author to whom any correspondence should be addressed.

the planned Einstein Telescope compared to current terrestrial gravitational-wave detectors.

Keywords: active vibration isolation, inertial sensing, voice coil actuation, cryogenics, vibration-free cooling, interferometry, gravitational-wave detection

1. Introduction

The Einstein Telescope (ET) [1–3] is the planned European third-generation ground-based gravitational-wave detector. Compared to currently operating second-generation detectors such as Advanced LIGO in the US [4], Advanced Virgo [5] in Italy and KAGRA [6–8] in Japan, ET aims for a sensitivity improvement of at least one order of magnitude over a wide frequency range and an extension of the detection band towards lower frequencies down to a few Hertz. ET will consist of nested pairs of detectors in a xylophone configuration [9], where each pair is formed by one detector optimised for low gravitational-wave signal frequencies (ET-LF) and one detector optimised for high signal frequencies. Especially ET-LF will require the development of new technologies, since it will operate at cryogenic temperatures as low as 10 K to reduce mirror coating thermal noise and suspension thermal noise, and it will use silicon as material for the mirror substrate and the final suspension stage.

In order to pave the way for ET-LF by testing new technologies and subsystems in a low-noise environment, a cryogenic prototype facility called ETpathfinder [10] is currently under construction hosted by Maastricht University, Netherlands. The facility is operated by more than 20 European research institutes and funded by a consortium of financial partners. The cryogenic system of ETpathfinder is designed such that it can operate at room temperature, at 123 K and at 10 K [11]. In gravitational-wave detectors, multi-stage pendulums are used in combination with sensors and actuators to decouple the interferometer optics from ground motion [12, 13]. ETpathfinder's cryogenic system is required to keep the mirrors stable at the above mentioned temperatures without introducing vibrations from the cooling system to the mirrors that exceed $10^{-18}\,\mathrm{m}\,\sqrt{\mathrm{Hz}}^{-1}$ above 10 Hz.

At ETpathfinder, the cool-down is initiated by a powerful liquid Nitrogen system that extracts hundreds of Watts to reach a temperature of 80–100 K. Additionally, a sorption-based chain of cryocoolers brings the system down to 10–20 K. The main part of the cooling is done radiatively by layers of cryoshields at different temperatures down to 15 K to avoid seismic shortcuts. However, the effectiveness of radiative cooling decreases with a decreasing temperature gradient between the cryoshield and the object to be cooled, the silicon mirrors. The last cooling step is therefore performed via conductive heat transfer from a thermal link called coldfinger (8 K) to the mirrors.

The connection between the coldfinger and the mirrors is made by soft ultra-pure aluminium wires. These so-called jellyfish wires do not connect directly to the mirrors but via a cold platform that cools the marionette and reaction mass of the seismic isolation system. Therefore, the mirror is strongly decoupled from vibrations of the coldfinger caused by ground motion and the cooling system. Preliminary investigations have shown that vertical vibrations from the coldfinger are the most critical degree of freedom, but do not limit the sensitivity of ETpathfinder if they do not exceed ground motion [14]. The operating Japanese gravitational-wave detector KAGRA [6–8], which uses a cryogenic system design relying on pulse-tube coolers, exhibits higher harmonics of vibrational peaks at the frequency of the cooler cycle in its sensitivity [15, 16]. To avoid this problem, ETpathfinder will feature low-vibration sorption-based cryocoolers. However, the design is still ongoing and the level of vibrations introduced by the last

cooling stage was unknown at the time of this study. It is therefore reasonable to investigate strategies to actively stabilise the coldfinger against vibrations introduced by the cryogenic system.

For this purpose, JPE has designed and manufactured a 3D cryogenic active vibration isolator (CAVI) whose performance is discussed in this paper. Development and test of the isolator was part of the ET Technologies project, in which scientific institutes and companies worked together in addressing technical challenges of ET, such as low-vibration cooling. JPE has successfully produced and tested a 1D version of the CAVI [17] and delivered a prototype version of the 3D isolator for testing at the ETpathfinder facility. Section 2 introduces the design of the 3D CAVI and the setup used for its qualification. Section 3 presents the active and passive performance of the device followed by a discussion in section 4.

2. Isolator and test setup design

2.1. Mechanical design

The 3D version of the CAVI under investigation combines three 1D units, each under an angle α of around 55° with respect to gravity, arranged symmetrically around the vertical axis (z). Each of the modules contains a nested two-stage suspension, see figure 1, where the first stage provides passive isolation of the payload m_p from ground motion x_g and the second stage is for inertial sensing by measuring relative motion $X = x_\mathrm{p} - x_\mathrm{s}$ between payload and sensor mass m_s. The device is mainly made of aluminium and designed to operate under UHV conditions with pressures lower than 10^{-9} mbar and cryogenic temperatures down to 4 K. Pairs of titanium struts with integrated flexures allow independent motion of the three axes and connect the payload mass of each module to a circular platform with a diameter of 40 mm onto which the coldfinger or any other mass to be stabilised can be mounted with three screws.

Each of the modules can be modelled as a coupled two-mass resonator. Since the effective payload mass m_p is about two orders of magnitude larger than the sensor mass m_s, the dynamics of the payload is only marginally influenced by the dynamics of the sensor mass represented by its mechanical transfer function $T^\mathrm{s}_\mathrm{ho} = x_\mathrm{s}/x_\mathrm{p}$, while the sensor mass is strongly influenced by the dynamics of the payload mass represented by the mechanical transfer function $T^\mathrm{p}_\mathrm{ho} = x_\mathrm{p}/x_\mathrm{g}$.

Above the sensor mass resonance $\omega_{0\mathrm{s}}$, the proof mass m_s is isolated from payload motion ($x_\mathrm{s} \approx 0$) and the sensor effectively measures payload motion x_p. Below its fundamental resonance, the proof mass will follow payload motion, the relative motion between proof mass and payload decreases with $1/\omega^2$ towards lower frequencies and the sensor effectively measures payload acceleration. The interferometric sensor readout of the CAVI detailed in section 2.2 is therefore sensitive to both payload acceleration $\ddot{x}_\mathrm{p}$ proportional to the force acting on the platform F_d and payload displacement x_p which are related but show different dependence on angular frequency ($\omega = 2\pi f$) as

$$T^\mathrm{s}_\mathrm{ho} - 1 = \frac{X}{x_\mathrm{p}} = \frac{\omega^2}{\omega_{0\mathrm{s}}^2 - \omega^2 + \mathrm{i}\frac{d_\mathrm{s}}{m_\mathrm{s}}\omega} = -\omega^2 m_\mathrm{p} \cdot \frac{X}{F_\mathrm{d}}. \tag{1}$$

In order to increase the sensitivity in the frequency range below the sensor mass resonance, the resonance frequency $\omega_{0\mathrm{s}} = \sqrt{k_\mathrm{s}/m_\mathrm{s}}$ should be minimised, for instance, by decreasing the ratio between the stiffness k_s and the sensor mass m_s while considering the space constraints related to the application. Decreased stiffness leads to a sag of the sensor mass due to its weight which needs to be compensated. For that purpose, JPE implemented a magnetic gravity compensation (MGC) which consists of adjustable permanent magnets introducing an effective

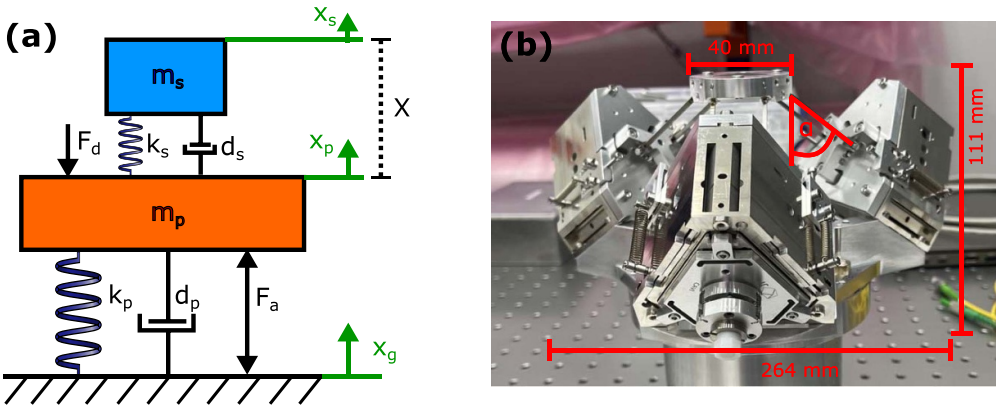

Figure 1. (a) Working principle of the 1D CAVI and (b) geometry of the 3D CAVI. Each of the three CAVI modules consists of an inertial sensor mass m_s with spring constant k_s and damping d_s on a payload mass m_p with spring constant k_p and damping d_p. This enables passive isolation from ground motion x_g above the resonance of the payload suspension. Interferometric sensing of $X = x_p - x_s$ enables additional active stabilisation from ground motion and disturbances F_d by means of actuator force F_a.

negative stiffness k_{mag} and a frequency-independent magnetic coupling of motion dominating the system dynamics below a certain frequency.

The 3D CAVI has a total mass of around 2.3 kg and would fit into a cylinder of a diameter of 265 mm and a height of 112 mm. It can support a wide range of payload masses (∼0.5–2.0 kg) utilising exchangeable tensile springs attached to the outside of each module to counteract the payload mass. For the purpose of qualifying the isolator for potential use as ETpathfinder cold-finger stabilisator, a copper bar of length 500 mm, width 30 mm and height 10 mm with total mass 1.28 kg was placed onto the CAVI platform. The dimensions were chosen to achieve a payload of mass and moment of inertia similar to the foreseen ETpathfinder coldfinger geometry. Additionally, a grid of holes was added to the copper payload to allow connection of cooling lines to the setup to measure levels of vibration introduced by the cryogenic system and vibration suppression capability by the 3D CAVI, once the design of the cryogenic system is completed.

2.2. Sensing and control

Active isolation is enabled via inertial sensing of motion along all three axes of the 3D CAVI X_{axi} with a commercial Displacement Measuring Interferometer (IDS3010) supplied by Attocube. The system features a compact, fibre-based, low-finesse Fabry–Perot interferometer. It sends out a stabilised laser source at 1530 nm wavelength which is frequency modulated at several MHz. Part of the laser light is reflected from the ferrule surface of the metric M12-sized collimator, which is screwed into the suspended payload of each CAVI module. The light exiting the sensor head is reflected off a mirror that is glued onto the suspended sensor mass. Adjustment screws in the sensor head mount enable tilt motion of the sensor head for alignment such that the reflected light is coupled back into the sensor head. The contrast of the interferometric readout of the individual sensor axes can be checked in the web interface that comes with the IDS3010 and needs to be between 20% and 80% for nominal operation according to the manufacturer. A higher interferometric contrast gives a higher signal-to-noise

ratio; however, due to the inherent sensitivity of the sensor to angular misalignment, optimal contrast cannot be guaranteed at all times.

The displacement signal from all three interferometric sensors is processed digitally and is converted into an analog signal for integration into the 18 bit data acquisition system of ETpathfinder, which is a copy of the DAQ-system used for sensing and control of the Virgo gravitational-wave interferometer [5]. For each axis, the 12 bit digital-to-analog converter of the IDS3010 signal processing unit produces differential signals in quadrature, i.e. proportional to sine ($V_{\mathrm{ax}i}^{\sin} \sim \sin(X_{\mathrm{ax}i}/R \cdot \pi/2)$) and cosine ($V_{\mathrm{ax}i}^{\cos} \sim \cos(X_{\mathrm{ax}i}/R \cdot \pi/2)$ of the relative displacement $X_{\mathrm{ax}i}$. The quarter wavelength R of these sine and cosine functions used to encode the displacement signal can be chosen in the resolution setting of the IDS3010 web interface. For the measurements described in the following sections on this paper, a resolution of $R = 10\,\mathrm{nm}/90^{\circ}$ was chosen as a trade-off between the risk of missing fringes, if the resolution is too small, versus the increase of the quantisation error, if the resolution is too large for the maximum expected payload speed at typical ground motion levels in the ETpathfinder cleanroom. The relative motion is reconstructed using a digital real-time computation of

$$X_{\mathrm{ax}i} = \frac{2R}{\pi} \cdot \arctan\left(\frac{V_{\mathrm{ax}i}^{\sin}}{V_{\mathrm{ax}i}^{\cos}}\right). \tag{2}$$

The inertial motion of the payload x_{p} can be recovered from this signal via plant inversion, that is, by multiplying with $\left(T_{\mathrm{ho}}^{\mathrm{s}} - 1\right)^{-1}$, see equation (1).

The motion measured per axis is fed back as an error signal to suppress vibrations using force F_{a} applied through JPE-supplied Cryo Voice Coil Actuators. These contactless, linear electromagnetic force actuators can operate down to 5 K and consist of an all-welded titanium construction hermetically sealing the coil to ensure UHV compatibility. They have a force response of 4 N/A in air at room temperature with a slight reduction to 3.83 N/A at 10 K. In this test, the coil driver was set to a maximum current of 4 mA, resulting in a peak force of 16 mN in ambient conditions.

For an out-of-loop measurement of payload motion, the shadow sensing of three Birmingham Optical Sensors and Electro-Magnetic actuators (BOSEMs) [18] was used to measure vertical motion at the ends of the copper bar and in its centre. This is motivated by vertical motion being previously identified as most critical since it couples the strongest to the cryogenic payload via the jellyfish wires [14]. Payload motion can be extracted from these relative sensors by plant inversion of the payload suspension with transfer function $T_{\mathrm{ho}}^{\mathrm{p}}$, that is, by multiplication with $T_{\mathrm{ho}}^{\mathrm{p}}\left(T_{\mathrm{ho}}^{\mathrm{p}} - 1\right)^{-1}$. The positioning of the sensors allows for readout of vertical motion, but also differential (pitch) and common (butterfly) vertical motion between both ends of the copper bar. Due to its geometry, the lowest resonance modes of the copper bar itself are expected to be around 100 Hz potentially disturbing active control of the translational degrees of freedom, which makes an additional readout beneficial.

An addition to shadow sensors, a compact broadband Trillium 120 (T120s) seismometer from Nanometrics was placed on the table to measure input ground motion. The velocity readout of the Trillium can be converted to displacement through division by the angular frequency $\omega = 2\pi f$. For direct comparison of motion in the different degrees of freedom, the coordinate system of the 3D CAVI needs to be aligned with the Cartesian coordinate system of the seismometer indicated in figure 2. Assuming that there is no significant cross-coupling between the axes, this can be done based on the geometry of the system by calculating the eigendirections of the 3D CAVI corresponding to the sensitive directions along its three axes. Matrix inversion of the matrix formed by the eigendirections gives the so-called sensing matrix

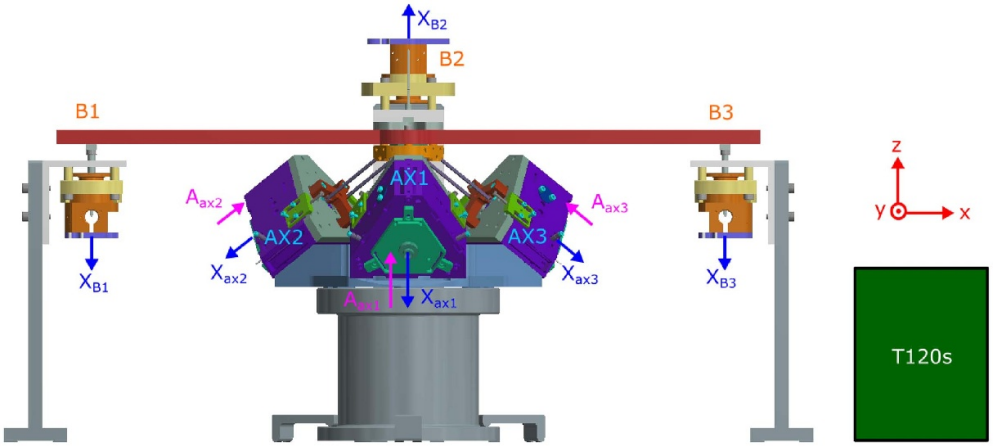

Figure 2. Schematic overview of the test setup including location of interferometric sensors AXi of the CAVI, geometric shadow sensors Bi and seismometer T120s. Sensor signals are denoted X_j (blue), feedback signals for active control are denoted A_j (pink).

of the 3D CAVI,

$$\begin{bmatrix} X_x \\ X_y \\ X_z \end{bmatrix} = \begin{bmatrix} 0 & -0.7071 & 0.7071 \\ -0.8164 & 0.4082 & 0.4082 \\ 0.5774 & 0.5774 & 0.5774 \end{bmatrix} \cdot \begin{bmatrix} X_{\mathrm{ax1}} \\ X_{\mathrm{ax2}} \\ X_{\mathrm{ax3}} \end{bmatrix}, \tag{3}$$

which converts motion signals measured along the three sensitive axes $X_{\mathrm{ax}i}$ $(i = 1,2,3)$ to motion in Cartesian degrees of freedom X_j $(j = x,y,z)$.

3. Isolation performance analysis

Passive isolation of the payload is achieved above 6.5 Hz by means of flexures inside the CAVI modules leading to a suspension with resonance frequency 4.8 Hz and measured quality factor of around 200. The payload suspension resonance shows slight variations up to ± 0.1 Hz between individual axes. The plant transfer function in figure 3 was measured by actuating with the voice coils along each individual axis with force $F_{\mathrm{a,ax}i}$[N] and measuring the response in the error signal $X_{\mathrm{ax}i}$[m] of each axis. In general, the behaviour of the plant can be described as a low-pass for disturbances such as ground motion or vibrations from the cooling system. Below a certain frequency, the coupling of the MGC dominates and the plant transfer function has a complex pair of zeros with $Q = 7$ at a frequency varying from axis to axis (0.53–0.8 Hz), where the coupling of the sensor mass suspension and the MGC compensate. The sensor mass suspension has its resonance frequency at 10.5 Hz for all three axes. The shadow sensor signals indicate that the antiresonance-resonance pair around 12.56 Hz stems from cross coupling of pitch motion, since only sensors B1 and B3 observe motion around that frequency. The origin of the strong resonance at 125.6 Hz is not completely understood and has not been observed in previous tests of the 1D isolator [17]. At this frequency, cross-coupling between all three axes and coupling to the shadow sensors is observed at similar levels as coupling to the actuation axis. From FEM analysis, the first mechanical resonance of the copper bar itself is expected to be around 101 Hz.

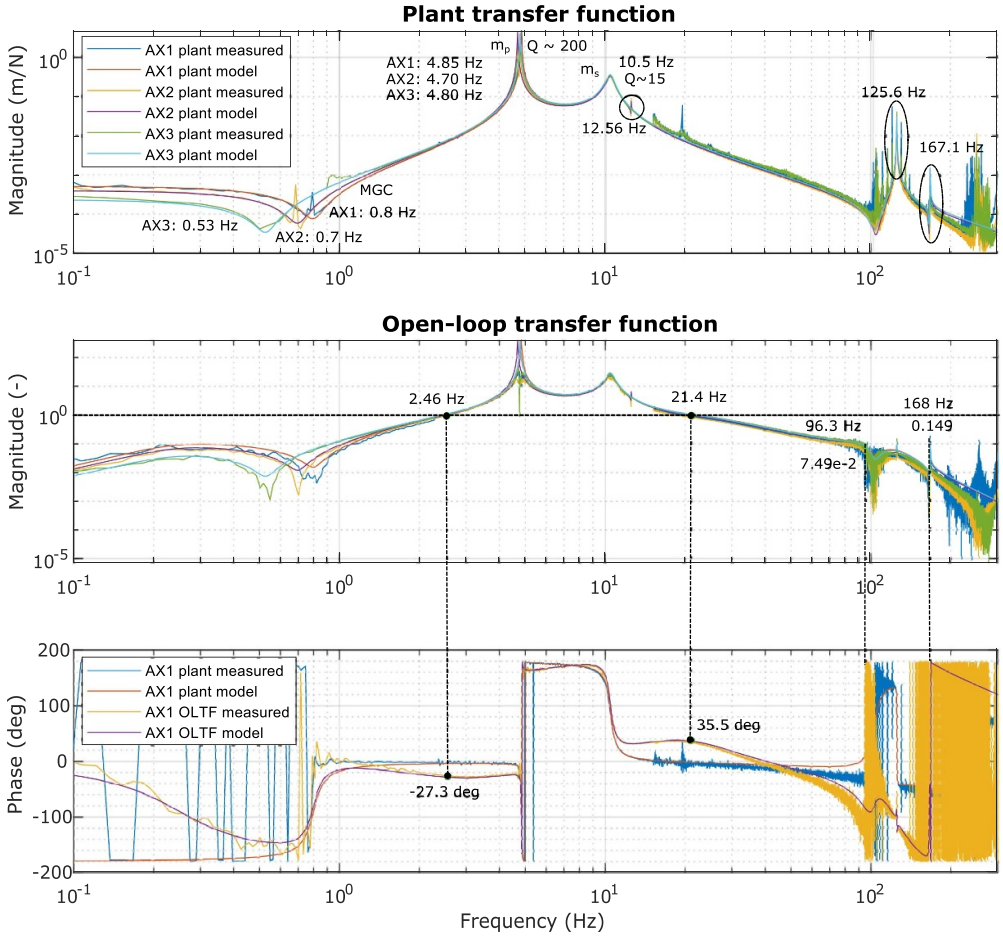

Figure 3. Measured and modelled plant (top) and open-loop transfer function (middle) for all three individual axes. Apart from slight frequency variations in the dip due to MGC (0.53–0.8 Hz) and the payload resonance (4.7–4.85 Hz), all three axes show very similar behaviour. Hence, the phase of both plant and open-loop transfer function (bottom) is only shown for AX1 for the sake of readability.

Since the requirement of the coldfinger is to move similarly to or less than the ground at all frequencies, active control needs to suppress the motion on the resonance of the passive isolator and attenuate excess motion from the sorption coolers. By extending the control band towards lower frequencies, the suppression of ground motion is improved similarly and thus gives a larger safety margin. A larger control bandwidth also allows active isolation to counteract possible disturbances from the cryogenic system directly acting on the payload, which might otherwise increase the motion of the coldfinger above ground motion. In this test specifically, the goal is also to explore limitations of the active control and investigate if it can be adjusted accordingly once the requirements are confirmed experimentally. The controller chosen for this application relies on phase-lag and phase-lead action to realise stable control around the two unity gain frequencies (UGFs) at 2.46 Hz and 21.4 Hz. Thus, the controller enables active suppression of disturbances between these two frequencies. Phase lag at the lower UGF is

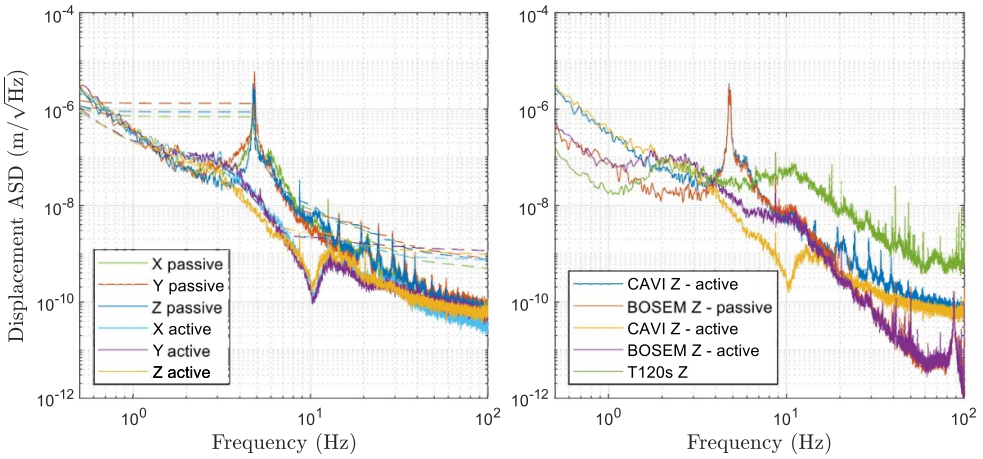

Figure 4. Left: Passive and active ASD of payload motion in the three Cartesian degrees of freedom measured by the 3D CAVI in a passive and active state. Dashed lines show the RMS motion. Right: Achievable motion in the vertical direction measured by the CAVI in the passive (blue) and active (orange) condition compared to the vertical motion measured by out-of-loop sensors. Geometric shadow sensors measure relative motion between ground and payload (red, purple), while the T120s seismometer measures vertical table motion (green).

introduced by a pole-zero combination at 2.4 Hz (pole) and 3.75 Hz (zero), phase lead at the higher UGF is achieved by a zero-pole combination at 15 Hz (zero) and 25 Hz (pole).

The digital controller is high-pass filtered with a complex pole at 0.25 Hz ($Q = 1$) to prevent large drifts. Towards lower frequencies, the controller design is limited by the coupling of the MGC. The digital controller is also low-pass filtered with a pole at 100 Hz to prevent sensor noise coupling at higher frequencies. The resonance structure at 125.6 Hz is filtered by means of an aggressive (broad) notch-filter using a complex zero of $Q = 250$ and a complex pole of $Q = 2.5$. In addition to the delay of the data acquisition system (700 μs), both the roll-off and the notch-filter required to prevent high-Q mechanical modes above 100 Hz from peaking through unity gain lead to phase loss that limits the control towards higher frequencies. Since the device is foreseen to operate at cryogenic temperatures, the resonance frequency of the notch-filter is expected to shift by tens of per cent towards higher frequencies at 10 K compared to operation at room temperature. Hence, the controller design is expected to be different for different operating conditions albeit maintaining the same control strategy.

Figure 4 shows the amplitude spectral density (ASD) of payload motion as measured by the 3D CAVI for the three Cartesian degrees of freedom (left plot). These spectra in units of $\mathrm{m}\sqrt{\mathrm{Hz}}^{-1}$ are obtained by measuring the error signal open-loop (passive) and closed-loop (active) and obtaining payload motion via plant inversion with the inertial sensing transfer function in equation (1) plus decomposition into Cartesian degrees of freedom using the sensing matrix in equation (3). This shows that the integrated root-mean-square (RMS) motion (dashed lines) can be reduced by one order of magnitude in the active control band due to active damping of motion around the payload resonance, which dominates the RMS motion in the passive case. The peaks present in the passive spectra are not real motion, but nonlinear upconversion of motion at the payload resonance during signal processing, hence, they disappear in the active case.

The right-hand side plot in figure 4 shows vertical motion measured by the 3D CAVI in the passive (blue) and active (orange) state compared to vertical payload motion as measured by the geometric shadow sensors in the passive (red) and active (purple) state. For reference, ground motion as measured by the Trillium seismometer (green) positioned next to the setup is also displayed showing that payload motion is suppressed below ground motion levels for frequencies above 4 Hz when the CAVI is actively controlled and approximately follows ground motion for frequencies 2–4 Hz. Note that the passive spectra were recorded early in the morning to reduce non-linearities from upconversion of motion around the payload resonance. The displayed ground motion spectrum (T120s) was recorded during office hours and represents ground motion levels during the measurement of active spectra with increased motion around 3 Hz due to anthropogenic activities. Since the interferometric sensors of the CAVI use the inertial sensor mass as a reference, motion around the sensor mass resonance is also suppressed leading to a dip in the displayed spectra. The spectra are limited by sensor noise above $\sim$20 Hz for the Attocube interferometric sensors and above $\sim$100 Hz for the BOSEMs.

4. Conclusion and outlook

In this paper, the passive and active performance achievable with the 3D CAVI designed and manufactured by JPE was investigated with the goal of evaluating its potential use as active isolator of the ETpathfinder coldfinger. The device provides passive isolation from ground motion above 10 Hz and additional active suppression of motion in the frequency band between 2.46 Hz and 21.4 Hz leading to a reduction of RMS motion by one order of magnitude in the active control band compared to purely passive isolation.

The interferometric sensor readout was found to be the most challenging part during commissioning and operation. Alignment of the sensors could be improved by means of having two alignment screws instead of three per axis to allow for separate alignment of the two degrees of freedom. Additionally, it could be investigated if a replacement of the mirrors on the sensor mass by retroreflectors would simplify the alignment by reducing sensitivity to angular misalignment while introducing sensitivity to lateral misalignment. However, space constraints and lateral dynamics due to tolerances in the sensor mass suspension need to be taken into account.

During the test, the 3D CAVI needed to be elevated with a cylindrical pedestal to avoid seismic shortcuts from the optical fibres on the table. This needs to be taken into consideration for future applications that require the 3D CAVI to sit on a surface larger than its contact surface, but is not expected to pose a problem for the ETpathfinder coldfinger isolation due to mounting prospects.

The frequency range and level of vibrations that will couple directly to the coldfinger via the cooling lines are currently unknown, but might require an extension of the active control bandwidth to both higher and lower frequencies. To enable this, current limitations like the MGC at low frequencies, but also sensor noise and the origin of the resonance at 125.6 Hz need to be investigated. The level of sensor noise might be dependent on the resolution setting in the IDS3010 which in turn is chosen to comply with the maximum expected payload speed occurring around the payload resonance at $\sim$4.8 Hz. For lower levels of input motion, it can be set to a lower value resulting in lower levels of sensor noise as demonstrated in a huddle test on the seismically isolated table at the AEI 10 m Prototype in Hannover [19]. This assumption can be tested once the setup is placed on the suspended bench of the ETpathfinder beamsplitter tower, which is under construction at the time of writing. If found to be true, the limitation can be overcome by choosing a readout mechanism that does not rely on digital pre-processing before

sending an analog signal to the ETpathfinder DAQ. In general, optical readout techniques like the Attocube interferometers introduce less sensing noise than capacitive or inductive readout methods [20]. However, the Attocube readout is not the most sensitive readout known in the gravitational-wave community, and a replacement by another readout, e.g. similar to the optical readout of the Cryogenic Superconducting Inertial Sensor [21], could be considered, if found to be compatible with the space constraints of the application.

In the future, operation of the 3D CAVI under UHV and cryogenic conditions should be investigated. Changes in the system dynamics under these operating conditions can be measured by a direct plant measurement before adjusting the control filters accordingly. Once a prototype of the ETpathfinder's sorption cooler is available, its connection to the coldfinger, vibration levels and the CAVI's capability to reduce them can be quantified. The CAVI reduces motion in the three Cartesian degrees of freedom but does not stabilise against tilt motion, which is known to limit the current seismic isolation of terrestrial gravitational-wave detectors [22]. Future research will show if an extension of the CAVI to a 6D system is required.

Data availability statement

The data that support the findings of this study are openly available at the following URL/DOI: https://doi.org/10.34894/PKFFEJ.

Acknowledgments

The authors would like to thank Bas Swinkels for useful discussions as well as Yves Israel (Ghent University) and Martin Adams (Nikhef) for production of mechanical parts. Part of this work was supported by Einstein Telescope Technologies project (OPZuid Project 03612) and the European Research Council (Advanced Grant 101019978). JL acknowledges support from the Deutsche Forschungsgemeinschaft (DFG, German Research Foundation) under Germany's Excellence Strategy-EXC-2123 QuantumFrontiers-390837967.

ORCID iDs

S L Kranzhoff 0000-0003-3533-2059
M J C Denissen 0009-0001-0261-0772
J Lehmann 0009-0000-6998-4413
B C T van Bree 0009-0002-5604-0784
M van Dael 0000-0002-6061-8131
M Vardaro 0000-0001-8604-3797
S Hild 0000-0001-9221-6009

References

[1] Punturo M *et al* 2010 *Class. Quantum Grav.* **27** 194002
[2] Maggiore M *et al* 2020 *J. Cosmol. Astropart. Phys.* JCAP03(2020)050
[3] Abac A *et al* 2025 The science of the einstein telescope (arXiv:2503.12263)
[4] Aasi J *et al* 2015 *Class. Quantum Grav.* **32** 074001
[5] Acernese F *et al* 2015 *Class. Quantum Grav.* **32** 024001
[6] Somiya K (the KAGRA Collaboration) 2012 *Class. Quantum Grav.* **29** 124007
[7] Aso Y, Michimura Y, Somiya K, Ando M, Miyakawa O, Sekiguchi T, Tatsumi D and Yamamoto H (The KAGRA Collaboration) 2013 *Phys. Rev. D* **88** 043007

[8] Akutsu T *et al* 2021 *Prog. Theor. Exp. Phys.* **5** 05A101
[9] Hild S, Chelkowski S, Freise A, Franc J, Morgado N, Flaminio R and DeSalvo R 2009 *Class. Quantum Grav.* **27** 015003
[10] Utina A *et al* 2022 *Class. Quantum Grav.* **39** 215008
[11] The ETpathfinder Team 2020 Etpathfinder design report (et-0011a-20) *Technical Report* (Maastricht University) (available at: www.etpathfinder.eu/wp-content/uploads/2020/03/ETpathfinder-Design-Report.pdf)
[12] Matichard F *et al* 2015 *Class. Quantum Grav.* **32** 185003
[13] Accadia T *et al* 2011 *J. Low Freq. Noise, Vib. Act. Control* **30** 63–79
[14] Utina A 2024 Instrumentation and characterization techniques for advanced gravitational-wave observatories *PhD Thesis* Maastricht University (https://doi.org/10.26481/dis.20241119au)
[15] Sakakibara Y *et al* 2014 *Class. Quantum Grav.* **31** 224003
[16] Bajpai R, Tomaru T, Kimura N, Ushiba T, Yamamoto K, Suzuki T and Honda T 2022 *Class. Quantum Grav.* **39** 165004
[17] Albers A *et al* 2023 *23rd Int. Conf. & Exhibition (Copenhagen, DK)* (available at: www.euspen.eu/knowledge-base/ICE23217.pdf)
[18] Carbone L *et al* 2012 *Class. Quantum Grav.* **29** 115005
[19] Kirchhoff R *et al* 2020 *Class. Quantum Grav.* **37** 115004
[20] Collette C, Janssens S, Fernandez-Carmona P, Artoos K, Guinchard M, Hauviller C and Preumont A 2012 *Bull. Seismol. Soc. Am.* **102** 1289–300
[21] Van Heijningen J *et al* 2022 *Nucl. Instrum. Methods Phys. Res. A* **1041** 167231
[22] Yu H *et al* 2018 *Phys. Rev. Lett.* **120** 141102